Prediction of rapid intensification of tropical cyclones with deep learning

---

This manuscript has been submitted for publication. The current version is a non-peer reviewed preprint submitted to EarthArXiv.

Authors and Affiliation

Sambatra Andrianomena[1,2], Mika Rafieferantsoa[3,*], Holifidy Rapanoël[3], and Rondrotiana Barimalala[4]

[1] South African Radio Astronomy Observatory (SARAO), Black River Park, Observatory, Cape Town, 7925, South Africa.

[2] University of the Western Cape, Bellville, Cape Town 7535, South Africa.

[3] A&A, Department of Physics, Faculty of Sciences, University of Antananarivo, B.P. 906, Antananarivo 101,
Madagascar

[4] University of Cape Town, Rondebosch, Cape Town 7701, South Africa.

*Corresponding author: rafieferantsoamika@gmail.com

Prediction of rapid intensification of tropical cyclones with deep learning

Sambatra Andrianomena[1,2], Mika Rafieferantsoa[3,*], Holifidy Rapanoël[3], and Rondrotiana Barimalala[4]

[1]South African Radio Astronomy Observatory (SARAO), Black River Park, Observatory, Cape Town, 7925, South Africa.
[2]University of the Western Cape, Bellville, Cape Town 7535, South Africa.
[3]A&A, Department of Physics, Faculty of Sciences, University of Antananarivo, B.P. 906, Antananarivo 101, Madagascar
[4]University of Cape Town, Rondebosch, Cape Town 7701, South Africa.
[*]Corresponding author: rafieferantsoamika@gmail.com

ABSTRACT

Tropical cyclones (TC) are one of the most destructive natural events claiming a lot of human lives and devastating coastal areas. Despite the advanced understanding of the formation of TC, prediction capabilities on the rapid intensification (RI) of TCs remain unsatisfactory. In this study, a deep learning framework using satellite images is used for the first time to identify RI events. We resort to the predictive power of VGG-like, ResNet-like and Xception architectures. The results show that the models are well capable of differentiating RI from non-RI events (*roc-auc* > 0.86), with a probability of detection (*POD*) > 0.83 and high fractional improvement over a random guess (*HSS*) > 0.57. The False Alarm Rate (*FAR*) is less than 0.23 on average. By considering only the best performance of the learners, *roc-auc* is maximized to 0.878 for VGG , 0.874 for ResNet and 0.911 for Xception; *FAR* decreases to 0.218 for VGG, 0.209 for ResNet and 0.182 for Xception, and *POD* are 0.864, 0.835 and 0.888 for the three models respectively. The trained models can be deployed in a real world scenario to help mitigate the further risks engendered by a TC going through a phase of rapid intensification.

Introduction

Predicting rapid intensification (RI) of tropical cyclones (TC) remains challenging due to the complexity of the factors controlling TC intensities and the limited understanding of meteorological covariates that best predict RI. Large-scale factors such as warm sea surface temperature, weak vertical wind shear, large upper-level divergence[1,2] as well as sub-surface ocean properties (e.g. upper-ocean heat content and barrier layer thickness[3]) are among the known mechanisms that can lead to an RI. There are cases when some of these factors are not fulfilled leading to unexpected RI[4]. However, rapidly intensified TCs, which are projected to increase in number[5], can lead to disastrous socio-economic consequences when there is a delay to inform and evacuate the affected areas.

In general, dynamical, statistical and hybrid statistical-dynamical models have been broadly used for RI prediction. Dynamical models are based on solving primitive equations and usually requires very high spatial resolution in order to represent the small scale features that impact the intensity of a TC. Despite the recent significant improvement in modeling techniques, physical parameterizations, computing resources as well as data availability for the model initialization, getting a better RI prediction remains a challenge by using dynamical models. On the other hand, statistical models are usually based on multiple regression techniques and assume a linear relationship between the predictors (e.g. large scale environmental variable) and predictand (e.g. intensity of a TC). Given the non linearity of the interaction of different processes that drive the intensification of a TC, skills of statistical models are also limited.

Recently, the weather prediction and TC research communities have started to make use of machine learning (ML) approaches to complement the standard methods. Pioneer works[6,7] used support vector machines (SVM) and logistic regression (LR) approaches. With synoptic-scale variables as predictors, SVM is found to outperform the LR model. Other methods such as artificial neural networks, and random forests were also used to generate RI forecasts[8]. The upper limits in the performance of these ML approaches exceed that of the standard methods. A more recent study[9] used the inner-core precipitation from satellite data, combined with other predictors employed by the US National Hurricane Center and found that their model outperforms the current standard operational methods. These studies suggest that overall, by using ML techniques together with different variables from satellite and reanalysis data as well as model outputs, there is a potential progress in the detection and prediction

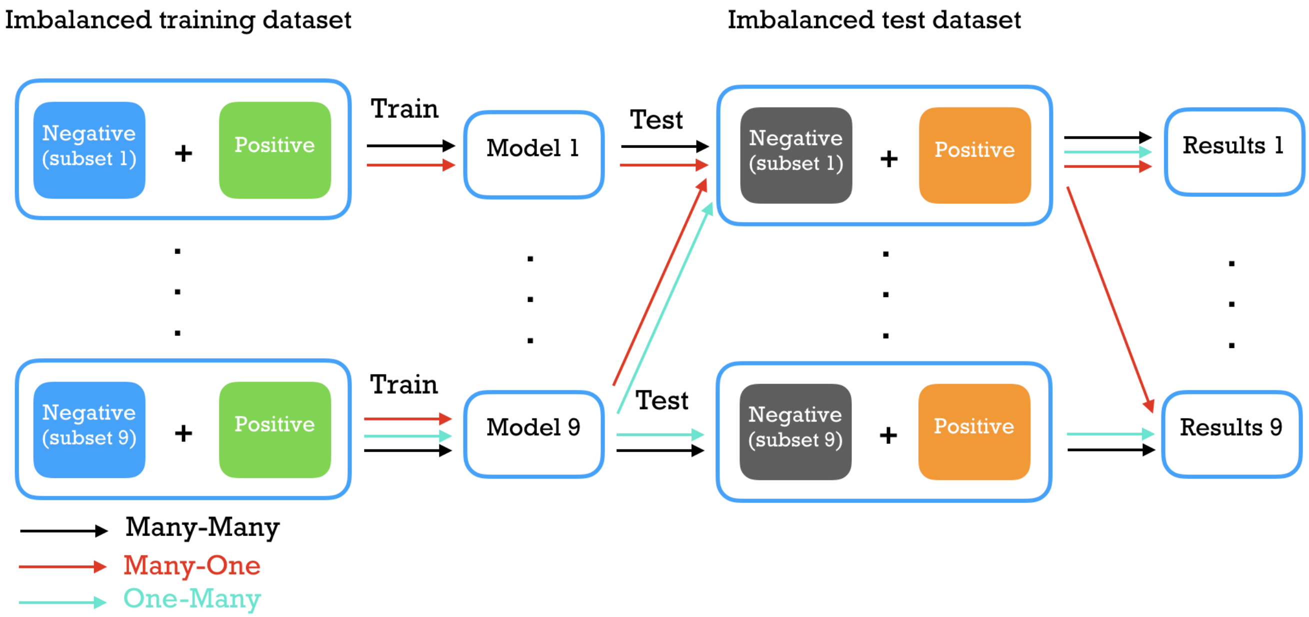

Figure 1. Training and testing configuration.

of RI. However, these models rely heavily on feature engineering and selection to identify the predictors that are most useful for prediction.
In this work, we develop a deep learning framework to identify RI from satellite images. Such framework allows us to better exploit the near real-time raw data by automatically learning discriminative features and to capture both spatial and temporal information from the highly resolved data. To the best of our knowledge, this is the first study that utilizes deep learning techniques to classify the rapid intensification of tropical cyclones.

Results

Using the HURSAT-B1 infrared temperature and sustained wind speed data, each time step in a given TC is labelled as RI or non-RI. A VGG-like, a Residual Network (ResNet) and an Xception models are then trained to predict the occurrence of an RI (See Methods for detailed description of data collection and processing, as well as network architecture). To deal with the effect of class imbalance, we adopt a data approach which consists of undersampling the majority class, i.e. the non-RI events. The idea is to randomly draw n instances from the negative class where n is the number of positive class in the training dataset. A balanced test set is obtained by using the same approach. To investigate the effect of the random sampling, the following three cases are considered (see Fig. 1)

- *many-many* case: it consists of running training-testing nine times using balanced dataset then averaging the considered metrics from all runs.
- *many-one* case: models are trained nine times with a balanced set whose negative examples are randomly drawn from the original dataset. At each training, the models are tested with the same balanced test set. The average value of each metric from all runs is then computed.
- *one-many* case: the model obtained from the best run – training that yields the best performance – is selected and tested with nine different test sets where the RI instances remain the same whereas non-RI event instances are randomly sampled from the original test set.

Table. 1 top panel shows the variations of all the performance measures selected in this work as a function of the runs in *many-many* setup. Results suggest that the randomly selected samples of negative class for both training and testing impact the performance of the classifiers. All metrics from each run fluctuate around the corresponding mean value (rather than constantly increasing or decreasing), implying that on average the three networks perform well. An average value of *roc-auc* ~ 0.86 denotes a good measure of separability. In other words, the probability that the networks are capable of differentiating the

Table 1. The performance metrics of the models from the three cases considered in this study.

	recall	*FAR*	*HSS*	*roc-auc*
		many-many		
VGG	$0.832^{\pm 0.059}$	$0.227^{\pm 0.030}$	$0.583^{\pm 0.015}$	$0.863^{\pm 0.007}$
ResNet	$0.838^{\pm 0.063}$	$0.234^{\pm 0.026}$	$0.578^{\pm 0.019}$	$0.862^{\pm 0.008}$
XCEPTION	$0.868^{\pm 0.056}$	$0.207^{\pm 0.026}$	$0.642^{\pm 0.030}$	$0.898^{\pm 0.007}$
		many-one		
VGG	$0.831^{\pm 0.059}$	$0.222^{\pm 0.027}$	$0.589^{\pm 0.016}$	$0.867^{\pm 0.005}$
ResNet	$0.838^{\pm 0.063}$	$0.231^{\pm 0.028}$	$0.581^{\pm 0.018}$	$0.864^{\pm 0.006}$
XCEPTION	$0.831^{\pm 0.070}$	$0.193^{\pm 0.037}$	$0.627^{\pm 0.031}$	$0.896^{\pm 0.005}$
		one-many		
VGG	$0.864^{\pm 0.000}$	$0.228^{\pm 0.007}$	$0.607^{\pm 0.010}$	$0.871^{\pm 0.008}$
ResNet	$0.835^{\pm 0.000}$	$0.216^{\pm 0.006}$	$0.604^{\pm 0.008}$	$0.870^{\pm 0.004}$
XCEPTION	$0.888^{\pm 0.000}$	$0.190^{\pm 0.007}$	$0.679^{\pm 0.010}$	$0.910^{\pm 0.003}$

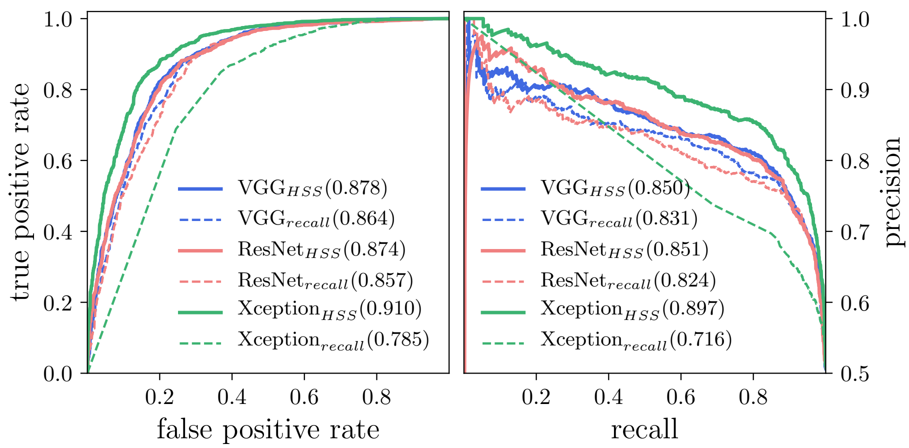

Figure 2. *roc* and *precision-recall* curves. Left panel shows *roc* curve which is the variation of the *true positive rate* as a function of *false positive rate*. Numbers in brackets are the values of the *roc-auc*. Right panel shows how the *precision* varies as a function of *recall*. *Average precision* is given by the area under the curve. In all cases blue, red and green lines correspond to VGG, ResNet and Xception respectively. Dashed lines indicate the results related to highest *recall* whereas solid lines are for best *HSS*.

positive from the negative class is about 86% (see Table. 1 top panel). Considering their ability to distinguish RI events from non-RI events, the networks are robust to the random change of the majority class in both the training and testing datasets, as evidenced by the relatively lower scatter, i.e. $\sigma_{roc-auc} < 0.009$.

The algorithms also exhibit good fractional improvements on a random guess, as suggested by the mean value of *heidke skill score* (*HSS*) > 0.57 (see Table. 1 top panel). Given that the main objective of this work is to predict whether a tropical cyclone at a specific time will go through a rapid intensification such that preventative measures can be taken accordingly, optimizing *recall* (or *POD*) (or minimizing False Negative) is of utmost importance. It is shown in Table. 1 top panel that compared to other metrics, *POD* varies within a relatively larger range with a standard deviation > 0.05, suggesting that it is more sensitive to the sub-samples used for both the training and testing. But overall, the probability of detection of the methods varies around 84%, indicative of a good performance of the learners. It is worth noting that *POD, HSS, FAR* are all based on a threshold value, above which an input is classified positive. Score can be the raw outputs from the network or a probability obtained by passing the network outputs through a SOFTMAX function. We recall that there is no activation function at the output layer of our networks. For deployment in a real world scenario, it is possible to adjust the threshold value such that the *recall*, under the assumption that it is the appropriate metric of the classification task, is increased. However in general, *sensitivity* is maximized to the detriment of *precision* (and vice versa); the so-called *precision - recall* trade-off. Hence, the adjustment of the threshold which aims to increase the probability of detection can be done at a fixed minimum value of *precision*, because a classifier with a relatively high *recall* but poor *precision* is not very useful. F_1 score, the harmonic mean of *precision* and *recall*, can

Table 2. The results corresponding to the types of best performance considered in *many-one*.

	recall	*FAR*	*HSS*	*roc-auc*
		High *HSS*		
VGG	0.864	0.218	0.622	0.878
ResNet	0.835	0.209	0.613	0.874
Xception	0.888	0.182	0.690	0.911
		High *recall*		
VGG	0.899	0.261	0.580	0.863
ResNet	0.934	0.283	0.565	0.856
Xception	0.981	0.409	0.303	0.757

be used as a good measure of the compromise between them. For the *many-many* case, we obtained an average value of F_1 score of $0.799^{\pm 0.015}$ with VGG, $0.798^{\pm 0.017}$ with ResNet and $0.827 \pm^{0.021}$ for Xception. These corroborate the fact that the classifiers perform reasonably well. Like *precision*, *FAR* is another indicator of the number of false positives. For an ideal case, *FAR* = 0 (or *precision* = 1). The percentage of false positives is minimized to around 0.227, 0.234 and 0.207 with VGG, ResNet and Xception respectively (see Table. 1 top panel). Although it is critical to optimize the probability of detection in this task, a relatively low value of *FAR* is beneficial since there are still some costs related to deploying resources in response to a "*false alarm*" in an environment with data-driven decisions. In this scenario, based on all four metrics, it is noticeable that the performance of Xception is better than those of the other methods. This trend is consistent with what was found on previous work[10] which compared their performance in a different classification problem.

Table. 1 middle panel shows the results from *many-one* setup. Its difference with *many-many* (Table. 1 top panel) is not considerable. Similar to *many-many*, *recall* fluctuates the most across the runs, as shown by the large standard deviation (> 0.05), and the dispersion of *roc-auc* remains small ($\sigma_{roc-auc} < 0.007$). In *one-many* scenario, the trained model obtained from the best run amongst the nine ones is tested on nine different test sets, each composed of the same positive class sample and a different negative class sub-sample at each run. Two ways of defining the best run for each model in *many-one* scenario are used; the training that corresponds to the highest *HSS* and the one achieving the highest *recall*. The results related to the highest *HSS* and *recall* are displayed in Table. 2 top and bottom panel respectively. It is shown that the *sensitivity* values are relatively higher (> 0.89) in the latter, denoting a minimized number of FN which is achieved at the cost of a higher FP as indicated by *FAR* > 0.26. However, a better generalization capability of the networks is apparent in Table. 2 top panel, despite the lower values of *recall* compared to those in Table. 2 bottom panel. This is supported by the larger value of *roc-auc* (> 0.87), higher fractional improvement over a random guess (*HSS* > 0.6) and a minimized FP (*FAR* < 0.22). Further comparison between the two types of best run can be done by taking into account the *average precision* which is defined as the mean of *precisions* computed for all possible values of threshold. It is found that the run with the highest *HSS* corresponds to *average precision* = 0.849, 0.850 and 0.897 for VGG, ResNet and Xception respectively, whereas the one with the highest *recall* yields *average precision* = 0.831, 0.823 and 0.716 for VGG, ResNet and Xception respectively. This confirms that high *HSS* value is indicative of a good predictive power in our task.

Fig. 2 shows the *roc* and *precision-recall* curves obtained from each network best run which is defined as the one with the highest *HSS* score (solid line) first then the one having the highest *recall* (dashed line) after. Based on the comparison between the two definitions of best performance in *many-one* scenario, we consider the trained networks with the highest fractional improvement to further investigate the impact of sampling in the *one-many* case. The results obtained from testing each trained model from the best run on nine different test sets are shown in Table. 1 bottom panel. The *recall* remains constant irrespective of the new sub-sample of negative class combined with the same positive class sample to form a *new* test set in each test. This is expected since the trained networks always identify/misidentify the same set of positive instances each time. It is noticeable that the scatter around the mean value of each metric is relatively smaller compared to those of the first two cases, *many-many* (Table. 1 top panel) and *many-one* (Table. 1 middle panel). This indicates that the classifiers are more sensitive to the dataset used for training. Overall, the Xception classifier, demonstrating better generalization capability, slightly outperforms the other two which exhibit similar performance. Lastly, it is noted that the inference time with an input image with 301×301 pixels is 12 ± 6ms on an Intel(R) Xeon(R) CPU E5-2690 v3 @ 2.60GHz.

Summary and Discussion

This work demonstrates the possibility of exploiting the predictive power of deep networks to predict whether a TC is going through a phase of rapid intensification using satellite images. To this end, we have made use of HURSAT-B infrared satellite images[11]. In this study, VGG-like, ResNet-like and Xception architectures are considered. An undersampling data approach is adopted in order to avoid the effect of the original imbalanced dataset on the classifiers performance. To highlight the effects of the undersampling, we have analyzed three different cases. Training/testing each model nine times with a different set of non-RI instances in the training/testing set each time (*many-many* case), running the training nine times with a different training set each time and testing the trained models from each run on a single balanced test set (*many-one* case), and finally testing each trained model corresponding to the best run on a different balanced test set (*one-many* case).

In the first case, *many-many*, the models demonstrate a great capability of distinguishing RI from non-RI events with a mean value of *roc-auc* > 0.86 and a relatively low standard deviation (≤ 0.008). This is consistent with the results obtained in previous studies[12] where they used a set of predictors (or features) such as the maximum intensity VMAX (see their Table. 1) as inputs using non-neural network methods which include Support Vector Machine, Naive Bayes, Logistic Regression and a tree based model; Classification And Regression Tree (CART). Their Logistic Regression attained a *roc-auc* = 0.89. Although it is not quite a fair comparison as the two approaches use two different types of inputs, the fact that our results slightly better than theirs is indicative of the great potential of the novelty of this work. The resulting mean value of *recall* > 0.83 suggests that each model is quite sensitive to the positive class, which is critical for predicting RI events. Our methods improve by a large fraction on a classifier with random guess as indicated by the average *HSS* > 0.57. A good generalization capability of an algorithm is characterized by optimized values of the metrics considered to assess its performance. In this work, identifying RI events is the main objective, nevertheless the ability of the classifiers to properly classify the negative instances is also of great interest. Together with the mean value of *roc-auc*, *recall* and *HSS*, the minimized mean value of *FAR* < 0.24 denotes that the classifiers generalize well.

It is found that the results obtained from both *many-many* and *many-one* are within the same ballpark, as evidenced by both the dispersion and the mean of each resulting metric value in each case. This suggests that the networks are less sensitive to different test sets, indicating a good fit. For the last case, *one-many*, the results highlight that in general a maximized fractional improvement implies optimized value of each metric, in contrast to the performance with the highest *recall*. Although the highest value of *POD* achieved are 0.899, 0.934 and 0.981 for VGG, ResNet and Xception respectively, the corresponding value of the other metrics is not optimized, such that the run that corresponds to the highest *HSS* is defined as the best.

Methods

Data collection and processing

This study makes use of global TC-centered geostationnary satellite imagery from the HURSAT-B1, with a particular focus on infrared temperature and sustained wind data set[11,13,14]. The initial data consists of 228,700 images of 3,790 TCs, which are globally distributed and span a 37-year period from 1980 to 2016. The evolution of each TC is recorded at a 3-hour interval. The data then consist of multiple instances or events per TC. The resolution of each image (at each event) is 301×301 pixels. An RI is characterized by an increase in sustained wind speed of 30kt – equivalent to 15m.s^{-1} – or more over a 24-hour period[2]. Each instance within a given TC is then labeled RI or non-RI accordingly as in a binary classification process. The given labels are matched to their corresponding two dimensional images which then become the input of the networks. It is noted that the RI events mostly occur by the first peak of the wind speed evolution. RI instances usually present a well-formed cyclone-like structure compared to their non-RI counterparts. Once trained, the networks predict whether the input is an image of positive class – an RI event – or not.

The data are split into training, validation and testing tests. Before splitting, the number of TCs with and without RI events are first balanced. Within the entire data, there are 557 TCs with at least one RI instance, and 3,233 TCs without RI. Out of the 3,233 non-RI TCs, we randomly select 557 to match its RI counterpart. After such reduction, a likelihood of 50% for a tropical cyclone to have at least one RI event during its lifetime is obtained. However in terms of the actual number of examples in each class, the dataset is still imbalanced as there are 7,498 RI events out of 68,984 instances ($\sim$1:9). To mitigate the effect of that bias towards the negative (non-RI) class, we opt for undersampling the latter such that the models are trained with well balanced datasets. A fraction of 20% of our data –14,845 instances – is set aside for testing. The remainder is further split into training and validation sets by 75% and 25% respectively, i.e. $\sim 46k$ instances for training and $\sim 15k$ for validation. To avoid any data leakage, the data are split by cyclone ordered by year. In other words, the training and validation sets consist of the first (by year) 80% of the data and the testing set the latest 20%.

Network architecture

In this work, three existing models are tailored to reach an optimal solution. In the first architecture, we leverage the higher capacity of a VGG-like architecture[15] to extract the relevant features. The key differences, compared to VGG-16, lie in the fact that instead of pooling, striding is used for downsampling, and the bias term is switched off in all layers. The extracted features are passed through three fully connected layers before the output layer. The second architecture consists of the network used in other study[16]. It results from the combination of a residual network (ResNet[17]) with inception modules[18]. In order to decrease the error, which deeper architectures are more prone to, the use of residual layers is proposed to improve the performance[17]. To learn from different scales at higher levels of the network, two inception modules are added after the last residual layer. The third architecture is the Xception model which inherits from the Inception structure where the modules are substituted with depth-wise separable convolutions[10]. That replacement made Xception outperform the Inception architecture on Imagenet data due to a more efficient use of the model parameters. We also exploit the capacity of Xception network in this study. The only modifications that have been implemented in the original architecture are the adaptation of the input layer to expect a 1 channel input, instead of 3, and the addition of a dense layer with one unit at the end of the chain to reflect our binary classification problem.

Performance measure

For easy reference, the four entries of a confusion matrix in a binary classification is defined as follows $\begin{bmatrix} TN & FP \\ FN & TP \end{bmatrix}$. Where, True Positive (TP) is the number of positive instances that are properly classified, True Negative (TN) is the number of negative instances that are well identified, False Positive (FN) is the number of negative instances that are misclassified as positive ones and False Negative (FN) is the number of positive examples that are identified as negative ones. To assess the performance of the methods, the following metrics are used

- *recall* also known as *probability of detection* (*POD*) or *sensitivity*. It denotes how well the classifier is able to minimize the number of positive instances identified as negative (false negative). It is given by

$$recall = \frac{\mathrm{TP}}{\mathrm{TP}+\mathrm{FN}}$$

- *Heidke Skill Score* (*HSS*) which indicates the improvement on a classifier with a random guess and reads

$$HSS = \frac{\mathrm{TP}\times\mathrm{TN}-\mathrm{FP}\times\mathrm{FN}}{(\mathrm{TP}+\mathrm{FN})\times(\mathrm{FN}+\mathrm{TN})+(\mathrm{TP}+\mathrm{FP})\times(\mathrm{TN}+\mathrm{FP})}$$

- *false alarm ratio* known as *FAR*, defined by

$$FAR = \frac{\mathrm{FP}}{\mathrm{FP}+\mathrm{TP}}$$

. A low value of this metric indicates a good classifier.

- *Receiving Operating Characteristic - Area Under the Curve (roc-auc)* is the result of averaging the variation of the true positive rate as a function of false positive rate. It indicates the degree of separability, in other words the capability of the model to distinguish between positive and negative examples.

References

1. Gray, W. M. Global view of the origin of tropical disturbances and storms. *Mon. Weather. Rev.* **96**, 669 – 700, DOI: 10.1175/1520-0493(1968)096<0669:GVOTOO>2.0.CO;2 (01 Oct. 1968).
2. Kaplan, J. & DeMaria, M. Large-scale characteristics of rapidly intensifying tropical cyclones in the north atlantic basin.

tropical cyclones in the south west
).1002/2016JC012028 (2017). https:

d intensification of tropical cyclones
ather. Rev. **146**, 3773 – 3800, DOI:

l physical environment. In: Managing
A Special Report of Working Groups I
ersity Press, Cambridge, UK, and New

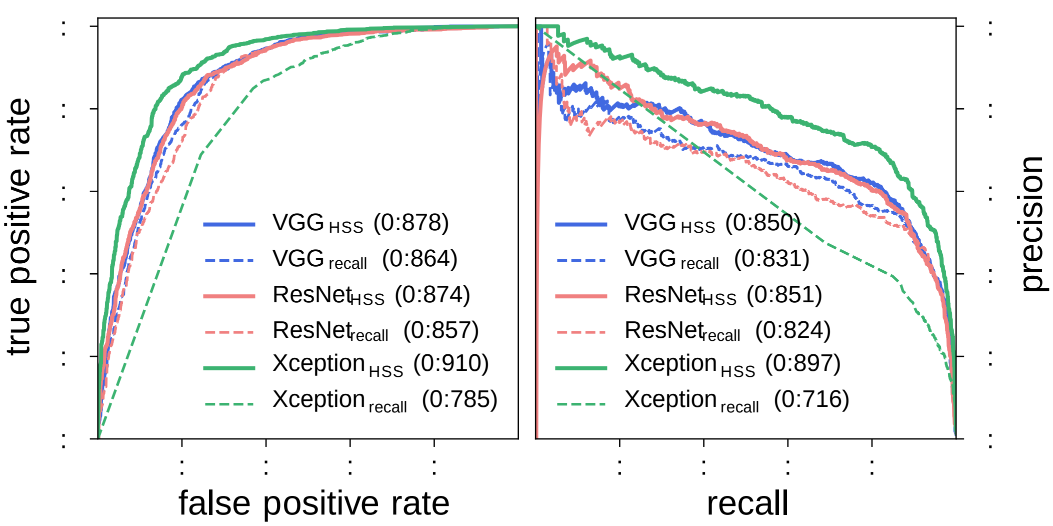

6. Grimes, A. & Mercer, A. E. Synoptic-scale precursors to tropical cyclone rapid intensification in the atlantic basin. *Adv. Meteorol.* **2015**, 814043, DOI: 10.1155/2015/814043 (2015).

7. Mercer, A. & Grimes, A. Diagnosing tropical cyclone rapid intensification using kernel methods and reanalysis datasets. *Procedia Comput. Sci.* **61**, 422–427, DOI: https://doi.org/10.1016/j.procs.2015.09.179 (2015). Complex Adaptive Systems San Jose, CA November 2-4, 2015.

8. Mercer, A. & Grimes, A. Atlantic tropical cyclone rapid intensification probabilistic forecasts from an ensemble of machine learning methods. *Procedia Comput. Sci.* **114**, 333–340, DOI: https://doi.org/10.1016/j.procs.2017.09.036 (2017). Complex Adaptive Systems Conference with Theme: Engineering Cyber Physical Systems, CAS October 30 – November 1, 2017, Chicago, Illinois, USA.

9. Su, H. *et al.* Applying satellite observations of tropical cyclone internal structures to rapid intensification forecast with machine learning. *Geophys. Res. Lett.* **47**, e2020GL089102, DOI: https://doi.org/10.1029/2020GL089102 (2020). https://agupubs.onlinelibrary.wiley.com/doi/pdf/10.1029/2020GL089102.

10. Chollet, F. Xception: Deep learning with depthwise separable convolutions. *CoRR* **abs/1610.02357** (2016). 1610.02357.

11. Knapp, K. R. & Kossin, J. P. New global tropical cyclone data set from ISCCP B1 geostationary satellite observations. *J. Appl. Remote. Sens.* 1 – 6 (2007).

12. Shaiba, H. & Hahsler, M. Applying machine learning methods for predicting tropical cyclone rapid intensification events. *Res. J. Appl. Sci. Eng. Technol.* **13**, 638–651 (2016).

13. Kossin, J. P., Knapp, K. R., Vimont, D. J., Murnane, R. J. & Harper, B. A. A globally consistent reanalysis of hurricane variability and trends. *Geophys. Res. Lett.* **34**, DOI: https://doi.org/10.1029/2006GL028836 (2007). https://agupubs.onlinelibrary.wiley.com/doi/pdf/10.1029/2006GL028836.

14. Knapp, K. R. Calibration assessment of isccp geostationary infrared observations using hirs. *J. Atmospheric Ocean. Technol.* **25**, 183 – 195, DOI: 10.1175/2007JTECHA910.1 (01 Feb. 2008).

15. Simonyan, K. & Zisserman, A. Very deep convolutional networks for large-scale image recognition. *arXiv preprint arXiv:1409.1556* (2014).

16. Hassan, S., Andrianomena, S. & Doughty, C. Constraining the astrophysics and cosmology from 21 cm tomography using deep learning with the ska. *Mon. Notices Royal Astron. Soc.* **494**, 5761–5774 (2020).

17. He, K., Zhang, X., Ren, S. & Sun, J. Deep residual learning for image recognition. In *Proceedings of the IEEE conference on computer vision and pattern recognition*, 770–778 (2016).

18. Szegedy, C. *et al.* Going deeper with convolutions. In *Proceedings of the IEEE conference on computer vision and pattern recognition*, 1–9 (2015).

Acknowledgements

S.A., M.R., H.R. and R.B. are thankful to Microsoft Azure for providing computing resources and technical supports. S.A. acknowledges support of the South African Radio Astronomy Observatory. R.B. was supported by the Royal Society FLAIR Program.

Author contributions statement

All authors contributed to the conception of the work, discussion of the results and the writing of the manuscript. S.A., M.R. worked on the network architectures and led the writing of the paper, H.R. worked on a code that was used for labeling the raw data. R.B. contributed on the climate science part of the work.

Additional information

Data availability
HURSAT-B1 data are freely available at `https://www.ncei.noaa.gov/data/hurricane-satellite-hursat-b1/archive/v06/`

Competing interests
Authors declare no competing interests. Correspondence and requests for materials should be addressed to M.R. (rafieferantsoamika@gmail.com). Reprints and permissions information is available at www.nature.com/reprints.